Cooling Dynamics of Individual Gold Nanodisks Deposited on Thick Substrates and Nanometric Membranes

Clément Panais, Romain Rouxel, Noëlle Lascoux, Sylvie Marguet, Paolo Maioli, Francesco Banfi, Fabrice Vallée, Natalia del Fatti, Aurélien Crut

Cooling Dynamics of Individual Gold Nanodisks Deposited on Thick Substrates and Nanometric Membranes

Clément Panais[1], Romain Rouxel[1], Noëlle Lascoux[1], Sylvie Marguet[2], Paolo Maioli[1], Francesco Banfi[1], Fabrice Vallée[1], Natalia Del Fatti[1,3] and Aurélien Crut[*1]

[1] Université de Lyon, CNRS, Université Claude Bernard Lyon 1, Institut Lumière Matière, F-69622 Villeurbanne, France

[2]Université Paris-Saclay, CEA, CNRS, NIMBE, 91191 Gif-sur-Yvette, France

[3] Institut Universitaire de France (IUF), France

Abstract

The cooling dynamics of individual gold nanodisks synthesized using colloidal chemistry and deposited on solid substrates with different compositions and thicknesses were investigated using optical time-resolved spectroscopy. Experiments demonstrate a strong substrate-dependence of these cooling dynamics, which require the combination of heat transfer at the nanodisk/substrate interface and heat diffusion in the substrate. In the case of nanodisks deposited on a thick sapphire substrate, the dynamics are found to be mostly limited by the thermal resistance of the gold-sapphire interface, for which a value similar to that obtained in the context of previous experiments on sapphire-supported single gold nanodisks produced by electron beam lithography is deduced. In contrast, the cooling dynamics of nanodisks supported by nanometric silica and silicon nitride membranes are much slower and largely affected by heat diffusion in the membranes, whose efficiency is strongly reduced as compared to the thick sapphire case. The dynamics are also affected by accumulation effects associated to the repeated character of pump pulse excitation, an effect negligible in the sapphire case. The time-resolved signals measured on membrane-supported nanodisks are analyzed in the framework of a finite-element thermal model operating in the frequency domain, from which the time-dependent temperature rise of a supported nanodisk heated by a periodic pulse train is deduced. This model allows for a good reproduction of the measured temperature evolutions, and enables an estimation of the values of both the thermal conductances of nanodisk-membrane interfaces and the thermal conductivities of the used membranes.

Understanding the specificities of nanoscale heat transfer is crucial for many technological applications. It is for instance essential in modern electronics for meeting the challenges set by the heating of densely packed nanometric transistors, for designing efficient nanostructured thermoelectric devices, or for developing imaging and therapeutic approaches exploiting the photothermal properties of nanoparticles.[1–4] Nanoscale heat transfer fundamentally differs from its bulk counterpart, in particular due to the increased role played by interfaces, which induce Kapitza resistances,[5,6] and because heat propagation becomes non-diffusive for systems with nanometric sizes of the order of (or smaller than) the characteristic dimensions ruling the thermal properties of bulk materials, such as their phonon mean free paths.[7,8] A large part of the current understanding of nanoscale heat transfer has been obtained using far-field optical pump-probe techniques working in the time or frequency domains.[9–11] These non-contact approaches rely on the selective heating of the absorbing parts of a sample using a pump pulse and on the optical monitoring of the induced thermal dynamics by a probe beam, whose propagation is modified by the pump-induced heating because of the temperature-dependence of the dielectric function of materials. This approach has for instance been successfully applied to study the thermal dynamics of bulk systems, layered structures and suspended nanometric membranes.[11–15]

Composite materials involving absorbing nanoparticles (e.g., metal ones) in a dielectric environment are highly relevant for investigating nanoscale heat transfer, as the heated and probed volumes in such experiments, set by the geometrical size of the used nanoparticles, can be much smaller than the diffraction-limited lateral size of optical beams (a few hundreds of nm). Evacuation of the energy optically injected in a nanoparticle away from it requires two successive processes: heat transfer at the interface between the nanoparticle and its environment, and heat propagation in the latter. The kinetics of these two processes (and therefore their relative contributions to the cooling dynamics) depend on many characteristics of the nanoparticle and of its environment, such as their thermal properties, morphologies, initial and transient temperatures, as well as on the nature of their interface. Depending on the investigated system, measurement of the cooling dynamics of metal nanoparticles is thus able to provide information about interface thermal conductances[16–21] (e.g., determining how their values depend on nanoparticle, environment and interface compositions) and/or about the modalities of heat conduction in the close environment of the nanoparticles[8,22–27], where Fourier's law can become invalid because of ballistic and hydrodynamic effects. The effect of high temperature rises, which may induce phase changes in either the nanoparticles or their environment, has also been addressed.[28,29] From the instrumental perspective, single-particle optical methods (which have already been largely used to study the linear optical response,[30,31] internal thermalization[32] and acoustic vibrations[33–36] of metal nano-objects)

have only been used at rare occasions in the field of nanoscale heat transfer.[37,38] They offer two major advantages over traditional ensemble experiments in this research area. The absence of averaging effects in single-particle experiments first allows to establish a finer connection between the composition and morphological features of the investigated systems and their thermal dynamics, as well as to characterize the reproducibility of these dynamics from one nanoparticle to another. Moreover, they also allow for a much more quantitative connection between thermal dynamics and their induced transient optical response, as the nanoparticle initial temperature rise and transient extinction changes can both be precisely quantified in these experiments.[38,39]

In this work, we apply single-particle time-resolved optical spectroscopy to the study of the cooling dynamics of individual gold nanodisks (NDs) supported on various dielectric substrates differing by their composition, thermal properties and thickness, and thus allowing a more or less efficient evacuation of heat away from the NDs. We investigate here the two extreme cases of NDs deposited on a thick crystalline substrate with high thermal conductivity (sapphire) and on nanometric, amorphous membranes with much lower thermal conductivity (silica and silicon nitride), the latter one corresponding to the original situation of a system where both the heater and its close environment have nanometric dimensions. By performing experiments on several individual NDs for each substrate, we characterize the reproducibility of ND cooling dynamics. Whereas the cooling dynamics of a ND deposited on a thick sapphire substrate are mostly ruled by interfacial heat transfer and near complete after ≈1 ns, those of NDs standing on suspended silica and silicon nitride membranes with 40-50 nm thicknesses are strongly influenced by heat conduction in the membrane and are much slower. Moreover, they turn out to be affected by the periodic character of ND excitation, achieved using a laser with 80 MHz repetition rate in our experiments. Indeed, the ND temperature rise prior to each new pump pulse, resulting from anterior pump excitations every 12.5 ns, is typically 10% of its maximal value in our experiments. The detailed analysis of the cooling dynamics of membrane-supported NDs is performed by finite-element modeling (FEM) in the frequency domain. This model allows for better understanding of the non-complete ND cooling before each pump pulse in the permanent regime. It also allows to quantitatively estimate the thermal conductances of ND/membrane interfaces and the thermal conductivities of the thin membranes in the vicinity of the NDs, used here as fitting parameters.

Gold NDs were prepared by colloidal chemistry, following an already published protocol.[40] Syntheses were performed in aqueous solution in presence of the cetyltrimethylammonium bromide (CTAB) surfactant. In a first step, gold nanoplates were obtained using a method initially proposed by Mirkin's group to produce triangular nanoplates.[41] A high percentage of hexagonal nanoplates (≈90%) was obtained to the detriment of triangular shapes (≈10%) by optimizing the concentrations

of the reactants in the growth solution, i.e. CTAB 0.1 M, $HAuCl_4$ 0.7 mM and ascorbic acid 1.6 mM. Au NDs were obtained in a second step, by mild oxidation of these hexagonal and triangular nanoplates smoothing their vertices and edges, using the Au(III)/CTAB oxidant complex, as explained elsewhere.[42,43] The morphological distribution of the Au NDs synthesized by this 2-step procedure was investigated using SEM imaging (Figure 1a), following ND deposition on an ITO substrate. Close to circular sections were observed for a majority of the produced nano-objects, a fraction of them however still presenting quasi-hexagonal or triangular sections. Statistics on the obtained SEM images yielded an average ND diameter of D=(97 ± 12) nm. The occasional observation of a few NDs contacting the substrate via their lateral surface rather than via one of their parallel bases also showed that their thickness h was of the order of 10 nm. A precise estimation of the average value of h could however not be performed using SEM, due to the weak number of NDs in this configuration and to uncertainties about their precise orientation. Deposition of the NDs for single-particle optical investigations was performed on three different solid substrates: a) a 480 µm thick (0001) α-Al_2O_3 (sapphire) single-crystal substrate, and b) 40 nm thick silica (SiO_2) and c) 50 nm thick silicon nitride (Si_3N_4) membranes patterned into 50 x 50 µm (silica) or 100 x 100 µm (silicon nitride) apertures etched in a 200 nm thick support mesh. The immobilization of NDs at the surface of these substrates was performed by depositing a drop of a very diluted solution of gold NDs which was left to dry, leading to a low density of deposited NDs (<1 ND/μm^2) as needed for performing far-field single-particle optical studies. Several copious ethanol rinsing followed by a UV/Ozone treatment were applied to remove any organic residues, as previously detailed in ref [44].

Localization and extinction spectroscopy of individual NDs immobilized on solid substrates were performed by spatial modulation spectroscopy (SMS), a far-field optical technique based on the periodic displacement of a sample illuminated by a tightly focused light beam, which induces a modulation of the transmitted light power when a nano-object is present in the light beam (Figure 1b).[30,45] An advantage of SMS is that the extinction cross-section σ_{ext} of single nano-objects can be quantitatively deduced from this modulated signal and measured as a function of the illumination wavelength λ and light polarization angle θ. SMS experiments were performed using a light source tunable over the 375−1040 nm wavelength range, obtained by combining a tunable femtosecond Ti:sapphire oscillator (producing λ=690-1040 nm pulses with f_{rep}=80 MHz repetition frequency) with a visible optical parametric oscillator and a frequency-doubling BBO crystal. The light beam delivered by this source was focused on the sample by a 100X microscope objective (with spot sizes on the sample of about 0.7 λ full-width at half-maximum, close to the diffraction limit), the direction of its linear polarization being controlled by a wire grid polarizer. Spatial modulation of the sample was performed at f=1.5 kHz frequency with 300 nm modulation amplitude and lock-in detection at 2f. In

this work, SMS was first used to localize individual gold NDs, which are randomly distributed over the substrate surface following the deposition step. Their σ_{ext} spectra presented a resonance associated to their in-plane dipolar surface plasmon resonance (SPR), with a central position λ_{SPR} varying from 700 to 900 nm. For some of the investigated nano-objects, a weak dependence of σ_{ext} on θ and a slight dipolar SPR degeneracy lift, signatures of a moderate in-plane morphological anisotropy[46], were observed (Figure 1b). Individual estimations of ND diameter D and thickness h were performed by comparing the central position and integrated spectral area of the quasi-Lorentzian experimental σ_{ext} spectra with those obtained in optical FEM simulations considering substrate-supported circular NDs (Figure 1b). D and h values respectively in the 85-115 nm and 7-12 nm ranges were deduced from this analysis for the investigated NDs. FEM modeling of extinction spectra thus leads to D values consistent with those deduced from SEM imaging of the synthesized NDs, while allowing a quantitative estimation of h.

The ultrafast dynamics of individual NDs were monitored using single-particle femtosecond pump-probe spectroscopy,[32,47] an approach based on the illumination of the investigated nanoparticle with two spatially overlapping, tightly focused and time-delayed femtosecond *pump* and *probe* light pulses (Figure 1c). Time-resolved measurements on individual NDs were practically performed by combining the SMS microscope with a two-color pump−probe setup based on the femtosecond laser source described above, delivering ~150 fs pulses. The oscillator pulse train was split in two parts to generate the pump and probe beams. In this work, a probe wavelength λ_{pr} close to λ_{SPR} was chosen for each investigated ND. This choice was based on previous numerical and experimental studies of the thermo-optical dynamics of single metal nanoparticles in dielectric environments.[38,48,49] Indeed, these investigations have shown that the sensitivity of time-resolved signals to nanoparticle heating is maximal when $\lambda_{pr} \approx \lambda_{SPR}$, while the contribution of environment heating to the measured signals simultaneously vanishes, ensuring specific probing of the nanoparticle temperature evolution. The probe beam was thus produced by the Ti:sapphire oscillator (with λ_{pr}=690-1040 nm), while second harmonic generation was used to generate the pump beam. Its fluence was tuned so as to limit the initial ND temperature rise to less than 20 K, as higher values were previously shown to lead to irreversible modifications of the ND optical response and cooling dynamics.[38] A mechanical chopper operating at 30 kHz was used to modulate the pump power. The pump-induced relative changes of probe beam transmission, $\Delta Tr/Tr$, were measured using synchronous detection as a function of the time interval separating pump and probe pulses, controlled by a mechanical delay line. This raw measured signal is directly related to the transient changes of the extinction cross-section $\sigma_{ext}(\lambda_{pr})$ of the investigated nano-object at probe wavelength λ_{pr} *via* $\Delta Tr/Tr = -\Delta\sigma_{ext}(\lambda_{pr})/S_{pr}$, with $S_{pr}=\pi d_{FWHM}^2/(4 \ln 2)$ the area of the probe spot and d_{FWHM} its full

width at half maximum.[32] As S_{pr} is an experimentally accessible parameter, these experiments provide access to the ultrafast variations of $\Delta\sigma_{ext}$ as a function of the pump-probe delay. To improve the signal to noise ratio, averaging over a few (from 2 to 10) successive pump-probe traces was performed, with optical realignments so as to maintain the pump and probe beams centered on the investigated ND.

The time-resolved signal measured on a single gold ND deposited on a 40 nm thick silica membrane is presented as an example in Figure 1c. This signal (as well as the other measured ones) exhibits two features which are typically observed in the context of time-resolved experiments on metal nanoparticles, namely an initial peak associated to the optical excitation and internal thermalization on few picosecond timescales of the ND and a relaxation on a nanosecond timescale, reflecting its cooling dynamics, i.e. the dissipation towards the environment of the energy deposited in the investigated nanoparticle by partial absorption of the pump pulse. Damped oscillations associated to ND acoustic vibrations were also apparent on some of the measured signals, but are hardly discernable in Figure 1c. The weak amplitude of the oscillatory component of the signals, associated to acoustic vibrations, is related to the choice of near-SPR probing, made, as discussed above, to specifically probe ND temperature dynamics. This is in agreement with previous investigations on metal nanospheres which showed that nanoparticle vibrations mostly induce a periodic SPR shift, and therefore a weak transient optical response at wavelengths close to the SPR central position.[35,50–52] Noticeably, the average signal value at negative time delays of the pump-probe trace presented in Figure 1c differs from zero, a feature indicating that the $T_{rep}=1/f_{rep}=12.5$ ns time separating two successive pump pulses is not sufficient for complete cooling of the ND (a complete modeling of this effect will be discussed below). The thermal components of the measured time-resolved signals, expected to be proportional to the ND temperature rise $\Delta T_{ND}(t)$ at times posterior to ND internal thermalization, were extracted from the raw signals by subtraction of their oscillating part (fitted using a sum of 1-3 damped sinusoids). They were additionally normalized so as to present the same value immediately after ND internal thermalization. The normalized $\Delta T_{ND}(t)$ dynamics deduced from this treatment show some variability from one ND to another (Figure 2a). However, for a given substrate, these normalized signals mostly differ by their average values at negative times (which ranges from 0 to 0.15 for all normalized signals). They present otherwise similar variations, as illustrated in Figure 2b which shows the normalized evolutions of $\Delta T'_{ND}(t)= \Delta T_{ND}(t)- \Delta T_{ND}(0^-)$, deduced from the signals of Figure 2a by subtraction of their average values at negative time delays $\Delta T_{ND}(0^-)$.

The normalized $\Delta T_{ND}(t)$ signals measured on thick sapphire substrate present the lowest value at negative times (<0.02 for all signals except one, for which the value is close to 0.1), indicating

that the cooling process is almost fully completed after T_{rep}, and that the periodic character of ND excitation by multiple pump pulses does not play an important role. The corresponding $\Delta T'_{ND}(t)$ signals present biexponential dynamics, with characteristic times $\tau_1 \approx 0.4$ ns and $\tau_2 \approx 50$-100 ps. Similar biexponential dynamics (with longer τ_1 and τ_2 characteristic times) were already observed in the context of previous time-resolved measurements performed on 18 nm and 40 nm thick gold NDs produced by electron beam lithography on a sapphire substrate.[38] The physical origin of the short exponential with characteristic time τ_2 still remains to be clarified, but the present work allows one to rule out an origin associated to a specific synthesis procedure (as it shows up for NDs synthesized by both lithography and colloidal chemistry). Moreover, we found that such a fast exponential appears in numerical models when considering a ND covered by a transparent impurity such as an ultrathin water layer, leading to a fast internal thermalization of the {ND-impurity} system following selective ND heating. As in our previous work,[38] we ascribe the monoexponential decay at delays exceeding 0.2 ns to ND cooling dynamics limited by heat transfer at the interface between the ND and its supporting sapphire substrate. The measured dynamics were similarly analyzed by comparing them with the simulated cooling dynamics of a ND following its excitation by a single pump pulse, using a complete thermal model considering both interfacial thermal resistance at the ND/substrate interface and diffusive heat propagation in the two media, leaving the interface conductance G as a free parameter. The modeled ND cooling dynamics being weakly sensitive to the thermal conductivity of the sapphire substrate, the bulk value of the latter was used, although previous studies suggest that its effective value near heaters of ≈100 nm lateral sizes may be reduced by ballistic effects.[8,26] The $\tau_1 \approx$ 0.4 ns measured cooling times were reproduced by using G ≈(65±10) $MW.m^{-2}.K^{-1}$ in the modeling, a value similar to the ≈(60±10) and (75±10) $MW.m^{-2}.K^{-1}$ ones obtained for the two samples of lithographed NDs investigated in our previous study.[38]

The cooling dynamics measured for NDs deposited on thin silica and silicon nitride membranes are close, and strongly differ from those of NDs deposited on thick sapphire substrates. They present larger normalized ΔT_{ND} values at negative time delays (Figure 2a) and non-exponential $\Delta T'_{ND}(t)$ dynamics which are much slower than in the sapphire case (Figure 2b). For instance, the time needed for $\Delta T'_{ND}$ decay down to 10% of its maximal value is about 3 times larger than in the sapphire case. The non-exponential decay of $\Delta T'_{ND}$ for NDs deposited on thin membranes implies that the cooling kinetics of membrane-supported NDs is not only ruled by interfacial heat transfer as in the thick sapphire case, and that heat propagation in the membranes is slow enough to strongly affect the observed dynamics. This large dissimilarity with the thick sapphire case originates from two distinct reasons making heat propagation in thin silica and silicon nitride membranes much less efficient than in a thick sapphire substrate. On the one hand, the thermal conductivities of silica and

silicon nitride are lower by about one order of magnitude than that of sapphire. On the other hand, heat diffusion in membranes away from a nano-heater becomes a two-dimensional process at time scales exceeding those required for heat to propagate over the membrane thickness. This greatly reduces the efficiency of heat spreading around the ND as compared to the case of thick substrates, where diffusion remains three-dimensional at all experimentally relevant time scales. Additionally, the non-vanishing normalized ΔT_{ND} values at negative time delays indicate that, conversely to the thick sapphire case, the time separating two successive pump pulses, T_{rep}=12.5 ns, is not sufficient for complete cooling of the NDs. This makes therefore their comparison with time-domain simulations involving a single pump pulse less relevant than in the bulk substrate case.

A modeling approach allowing, in the linear regime, to compute the thermal dynamics of a membrane-supported ND for any time-dependent heating process, was thus performed in this work. This approach was largely inspired by previous works in the field of time-domain thermoreflectance.[13,53,54] Its main idea consists in first calculating the complex frequency-domain response $\tilde{h}(f)$ of the investigated system, whose modulus and argument respectively describe the amplitude and phase of the system temperature oscillations with respect to a time-harmonic heating at frequency f. The Fourier transform $\widetilde{\Delta T}(f)$ of the thermal dynamics induced by any time-dependent excitation process $q(t)$, of Fourier transform $\tilde{q}(f)$, is then given by $\widetilde{\Delta T}(f) = \tilde{h}(f)\tilde{q}(f)$, allowing to deduce the corresponding temporal dynamics $\Delta T(t)$ by reverse Fourier transform.

In this work, the frequency-domain response $\tilde{h}(f)$ of a gold ND supported by a thin membrane was first calculated using FEM, based on the model described in Figure 3a. The modeled geometry consists of a cylindrical gold ND with diameter D and thickness h deposited on a cylindrical membrane characterized by its diameter D_m (with D_m>>D) and thickness h_m. The ND and membrane were described by their specific heats c_m (2.49, 1.59 and 2.13 MJ.m^{-3}.K^{-1} values being used for Au, SiO_2 and Si_3N_4) and thermal conductivities Λ_m (assumed to be isotropic). Bulk thermal conductivities values, 317 and 1.4 W.m^{-1}.K^{-1}, were used for Au and SiO_2. The high thermal conductivity of gold ensuring a quasi-uniform temperature within the ND at experimentally relevant timescales/frequencies, its precise value has little impact on the model predictions. Regarding silica, our choice was based on previous measurements which showed that the thermal conductivity of >25 nm thick silica films remains close to the bulk Λ_m value at room temperature,[12,53] as expected for a membrane thickness much greater than the phonon mean free path in silica (≈1 nm). Conversely, Si_3N_4 heat conductivity was left as a free parameter of our model, as room-temperature measurements on silicon nitride samples have led to very scattered Λ_m values (ranging from 0.3 to 10 W.m^{-1}.K^{-1}) in the past.[55–60] Thermal interface conductance values at Au-SiO_2 and Au-Si_3N_4 interfaces

were also left as free parameters. Sinusoidal energy injection (with frequency f) in the ND was considered. Thermal insulation boundary conditions were applied on the upper and lower circular bases of the cylindrical membranes, and constant temperature ones on their lateral surface (allowing a thermal flux out of the simulation system, which is important for avoiding divergence of ND temperature). 2D axisymmetric simulations exploiting the rotational symmetry of the considered geometry were performed, allowing to greatly reduce the required computational times. The spatial profile of the temperature rise (modulus) computed for a D=100 nm, h=10 nm gold ND located on a thin silica membrane with D_m=2 µm and h_m=40 nm when f=f_{rep} is shown as an example in Figure 3b.

It should be noted that the system considered in the simulations differs from the actual experimental configuration. Contrary to the simulation case, where a ND at the center of an homogeneous, 2 µm diameter cylindrical membrane is considered, in our experiments NDs are located at various positions on large square membrane windows (50 and 100 µm side length for silica and silicon nitride membranes, respectively). Moreover, the present model neglects heat dissipation to the surrounding air, a phenomenon whose efficiency is low for bulk systems (the convective heat transfer coefficient being of the order of 10 $W.m^{-2}.K^{-1}$ for natural convection in air, i.e., more than 10^6 times smaller than typical G values) but which may become more significant for micro- and nanometric systems, and has been previously demonstrated to influence the thermal dynamics of some suspended 2D systems.[61–63] Nevertheless, these differences between the systems considered in experiments and simulations are not relevant here because, as discussed below, they only affect the ND temperature rise preceding each pulse (Figure 2a), which presents large variations from one ND to another and that we did not attempt to quantitatively model, but not the $\Delta T'_{ND}(t)$ cooling dynamics obtained after subtraction of this offset value (Figure 2b).

The results of frequency-domain FEM simulations performed for the reference case of a D=100 nm, h=10 nm gold ND located on a thin silica membrane with D_m=2 µm diameter and h_m=40 nm thickness are shown in Figure 3c. The computed response globally evokes that of a low-pass filter, with the amplitude of the response being constant at low frequencies and decaying at high ones, and the phase shift between the excitation and the response going from 0 at low frequencies to $-\pi/2$ values at high ones. In order to clarify the influence of the key parameters of our thermal model on this frequency reponse, FEM calculations were reproduced with modified values of the interface conductance (G) and of some of the membrane characteristics (Λ_m, D_m and h_m) (Figure 3c). The induced changes of the response function are also shown in Figure 3d. As can be seen on this figure (and as previously noticed in the context of thermoreflectance investigations on thin films[54,64]), the sensitivities to interface and membrane characteristics have a different frequency dependence, which is essential to allow their independent determination. For a membrane-supported ND, the

low-frequency part of the response function mostly depends on membrane geometrical and thermal characteristics, while its high-frequency component is essentially sensitive to G value. This can be ascribed to the fact that temperature oscillations in the membrane occur on a smaller volume as frequency increases, giving more importance to interfacial effects.

The effect of G, which takes place over a broad frequency range, can be better understood by considering the simplified case of isothermal ND and membrane (obtained in the limit of very high membrane conductivities, and thus strongly differing from the situation addressed in Figure 3). The ND temperature evolution $\Delta T_{ND}(t)$ for a sinusoidal heating A exp(iωt) (with $\omega=2\pi f$) is then described by the differential equation $c_{Au}V\, d\Delta T_{ND}/dt+GS\Delta T_{ND}=A\exp(i\omega t)$ with c_{Au}, V and S the ND volumetric heat capacity, volume and surface in contact with the substrate (with V/S=h). The response function is in this case a low-pass filter one, $\tilde{h}(f) \propto \frac{1}{G}\frac{1}{1+i2\pi\tau f}$, with $\tau = hc_{Au}/G$ (=0.25 ns in the reference case considered in Figure 3), whose low-frequency limit and cutoff frequency $f_c=1/(2\pi\tau)$ are both affected by G, which thus impacts the response function over a broad frequency range (frequencies of the order of and below f_c).

It can also be observed in Figure 3 that membrane characteristics (Λ_m, h_m and D_m) affect the response function a different way, the effects of a reduction of h_m and D_m by a factor of 2 as compared to the reference case being in particular limited to the <1 GHz and <5 MHz frequency ranges, respectively. The existence of such frequency thresholds for the effects of h_m and D_m can be understood by considering the frequency-dependent thermal penetration length in a material $L_p = \sqrt{\frac{\alpha_m}{\pi f}}$, with $\alpha_m = \Lambda_m/c_m$ the membrane diffusivity (α_m=9 10^{-7} m^2/s for silica).[65] The finite thickness of the membrane thus has an influence at frequencies low enough for h_m to be smaller than L_p, i.e. for $f<\alpha/(\pi\, h_m^2)$ (about 200 MHz and 800 MHz for the 40 nm and 20 nm thicknesses considered in Figure 3cd, respectively). This simple analysis thus explains why the 2x reduction of h_m investigated in Figure 3cd is without effect at >1 GHz frequencies. It also predicts a non-negligible effect of h_m on the ND temperature dynamics in our experiments, which involve a periodic excitation with 80 MHz frequency. A similar analysis shows that the lateral size of the membrane impacts the response function only at frequencies lower than about 4 MHz for D_m=1 µm, making a decrease of D_m from 2 to 1 µm without effect for frequencies exceeding a few MHz (Figure 3cd).

The ND excitation process in our time-resolved experiments involves several very different time scales, ranging from ≈10^{-13} s (duration of pump pulses) to ≈10^{-5} s (pump beam modulation) which are however not all relevant to describe the measured ND temperature evolution. On the one hand, modulation of the pump beam being performed at a low frequency (30 kHz), more than 2000 times smaller than the repetition frequency of the used laser source (80 MHz) in our experiments, its

effect was neglected in the model. This simplification was supported by the absence of significant difference between time-resolved signals measured on a given ND using different modulation frequencies. On the other hand, the duration of the used laser pulses (≈150 fs) and that of internal ND thermalization by energy exchanges between electrons and ionic lattice (about 1 ps)[39] being both much smaller than the characteristic times of nanodisk cooling, excitation by each pump pulse was supposed to be instantaneous. We therefore considered a ND excitation process described in the time domain by a periodic train of delta pulses : $q(t) \propto \sum_{n=-\infty}^{+\infty} \delta(t - nT_{rep})$, to which is associated the Fourier transform $\tilde{q}(f) \propto \sum_{n=-\infty}^{+\infty} \delta(f - nf_{rep})$. The temporal evolution of ND temperature rise following each pump pulse, in the reference case of Figure 3cd and for modified values of G, Λ_m, h_m and D_m is presented in Figure 3e. $\Delta T'_{ND}(t)$ signals obtained after subtraction of the value at $t=0^-$ (i.e. the same treatment as in the case of experimental signals, to go from Figure 2a to Figure 2b) are shown in Figure 3f. Results obtained by time-domain simulations with a single pump pulse are also shown for comparison. While the main effect of a periodical ND excitation is a non-vanishing $\Delta T_{ND}(0^-)$ value, the $\Delta T'_{ND}(t)$ signals obtained for excitation by single (gray line in Figure 3f) and multiple pump pulses (black line in Figure 3f) also differ at timescales exceeding 1 ns, justifying the use of the complete model presented here to analyze our experimental results (note that the discrepancy between the two signals would be greater for membranes thinner than those considered in this work). G, Λ_m and h_m are shown to impact the normalized signals both before and after offset subtraction, while D_m only affects the offset value. This can be easily understood from the frequency-domain investigations discussed above, as D_m has an impact only at frequencies much smaller than f_{rep}, while excitation is performed with frequencies multiple of f_{rep} (see $\tilde{q}(f)$ expression above). Therefore, D_m only affects the zero-frequency component of the dynamics, i.e. the average ND heating. Conversely, G, Λ_m and h_m affect not only the average temperature rise, but also (and in different ways) the $\Delta T'_{ND}(t)$ cooling dynamics as they impact the response function at many frequencies multiple of f_{rep}. The average ND temperature rise is thus sensitive to the far environment of the NDs while, conversely, the normalized cooling dynamics $\Delta T'_{ND}(t)$ after offset subtraction is affected only by the characteristics of the close environment of the ND, i.e. in the small region around the ND where thermal energy penetrates at f_{rep} frequency (Figure 3b). Therefore, the $\Delta T'_{ND}(t)$ dynamics can be quantitatively analyzed even without precise knowledge of the membrane geometry and thermal properties over large scales.

A direct comparison between measured and modeled $\Delta T'_{ND}(t)$ dynamics is shown in Figure 4, for the two membranes considered in this work. As the signals measured on each membrane for different NDs were very similar, they were collectively compared to simulations performed for a D=100 nm, h=10 nm ND, i.e., D and h values close to the average ones determined using SEM

imaging and/or FEM modeling of extinction spectra. The cooling dynamics of NDs deposited on a 40 nm thick silica membrane were well reproduced using G=120 $MW.m^{-2}.K^{-1}$ together with the Λ_m value of bulk silica (Figure 4a). This G value stands at the upper end of the 40-140 $MW.m^{-2}.K^{-1}$ range of G values obtained for gold-silica interfaces in previous measurements and atomistic simulations[66–69], which have also shown a large dependence of G on silica growth procedure and crystalline or amorphous character. The determined G value is also close to the G=105 $MW.m^{-2}.K^{-1}$ one that we previously obtained in the context of thermal measurements on ensembles of gold nanospheres embedded in a glass with a large silica content.[70] The cooling dynamics of NDs deposited on a 50 nm thick silicon nitride membrane were also well reproduced by our simulations using slightly different parameters as in the silica case, namely G=150 $MW.m^{-2}.K^{-1}$ and Λ_m =1 $W.m^{-1}.K^{-1}$ (Figure 4b). Here too, the deduced values of G and Λ_m are compatible with previous reports. Indeed, the deduced G value is close to the only (to our knowledge) value reported in the literature for Au/Si_3N_4 interfaces, G=120 $MW/(m^2.K)$[71], while the Λ_m value used for fitting our data falls within the broad 0.3-10 $W.m^{-1}.K^{-1}$ range of previous measurements on silicon nitride membranes with different stoichiometries and thicknesses.[55–60] The proximity of the G and Λ_m values that we used for reproducing the $\Delta T'_{ND}(t)$ dynamics on silica and silicon nitride membranes reflect the similarity of the experimental signals measured on these two membranes, whose thicknesses are also close. Not taking into account the periodical character of the excitation, which affects the $\Delta T'_{ND}(t)$ dynamics (Figure 3f), would have translated into slightly different (by about 15%) optimal values of the fitting parameters G and Λ_m.

In conclusion, the large substrate-dependence of the cooling dynamics of single supported nano-objects was demonstrated in this work, which considered the extreme cases of both a thick substrate with high thermal conductivity and that of thin membranes with low conductivity. In the former one, the cooling dynamics were fast, quasi-exponential and mostly limited by the Kapitza thermal resistance of the nano-object-substrate interface, whose value was found to be close to that previously determined for gold NDs lithographed on sapphire, despite completely different ND synthesis and deposition procedures. In the case of membrane-supported NDs, the cooling dynamics were much slower and strongly non-exponential, demonstrating a large impact of membrane heat diffusion on these dynamics. A numerical model accounting for the repetititive character of nano-object excitation in the context of optical time-resolved experiments was developed and used to understand the dependence of the cooling dynamics on the different substrate properties and to quantitatively model the measured signals. In particular, a small membrane thickness was shown to greatly slow down the cooling dynamics at time scales exceeding those needed for heat to propagate over its thickness. Possible extensions of this work include the realization of more systematic investigations of the membrane thickness effect and the use of ultrathin or highly conductive

membranes, whose thermal conductivities may depend on their thickness or even be inaccurately described by Fourier's law of heat diffusion. Directly probing the thermal dynamics of the membranes (rather than that of the supported nano-objects) by adequate tuning of the probe wavelength would also be interesting to further clarify the modalities of heat propagation in the close vicinity of a nano-heater.

AUTHOR INFORMATION

Corresponding author

*****E-mail: aurelien.crut@univ-lyon1.fr

ORCID

Romain Rouxel : 0000-0003-2982-5818

Paolo Maioli: 0000-0002-4199-8810

Sylvie Marguet: 0000-0002-8670-1320

Francesco Banfi: 0000-0002-7465-8417

Natalia Del Fatti: 0000-0002-8074-256X

Aurélien Crut: 0000-0003-2185-709X

Notes

The authors declare no competing financial interest.

ACKNOWLEDGEMENTS

This work was supported by the French National Research Agency (ANR) under the reference *ANR-20-CE30-0016* (ULTRASINGLE project).

REFERENCES

(1) Cahill, D. G.; Ford, W. K.; Goodson, K. E.; Mahan, G. D.; Majumdar, A.; Maris, H. J.; Merlin, R.; Phillpot, S. R. Nanoscale Thermal Transport. *J. Appl. Phys.* **2003**, *93*, 793–818.

(2) Cahill, D. G.; Braun, P. V.; Chen, G.; Clarke, D. R.; Fan, S.; Goodson, K. E.; Keblinski, P.; King, W. P.; Mahan, G. D.; Majumdar, A.; Maris, H. J.; Phillpot, S. R.; Pop, E.; Shi, L. Nanoscale Thermal Transport. II. 2003–2012. *Appl. Phys. Rev.* **2014**, *1*, 011305.

(3) Pop, E.; Sinha, S.; Goodson, K. E. Heat Generation and Transport in Nanometer-Scale Transistors. *Proc. IEEE* **2006**, *94*, 1587–1601.

(4) Snyder, G. J.; Toberer, E. S. Complex Thermoelectric Materials. *Nat. Mater.* **2008**, *7*, 105–114.

(5) Swartz, E.; Pohl, R. Thermal Boundary Resistance. *Rev. Mod. Phys.* **1989**, *61*, 605–668.

(6) Stoner, R. J.; Maris, H. J. Kapitza Conductance and Heat Flow between Solids at Temperatures from 50 to 300 K. *Phys. Rev. B* **1993**, *48*, 16373–16387.

(7) Chen, G. Nonlocal and Nonequilibrium Heat Conduction in the Vicinity of Nanoparticles. *J. Heat Transfer* **1996**, *118*, 539–545.

(8) Siemens, M. E.; Li, Q.; Yang, R.; Nelson, K. A.; Anderson, E. H.; Murnane, M. M.; Kapteyn, H. C. Quasi-Ballistic Thermal Transport from Nanoscale Interfaces Observed Using Ultrafast Coherent Soft X-Ray Beams. *Nat. Mater.* **2010**, *9*, 26–30.

(9) Schmidt, A. J.; Cheaito, R.; Chiesa, M. A Frequency-Domain Thermoreflectance Method for the Characterization of Thermal Properties. *Rev. Sci. Instrum.* **2009**, *80*.

(10) Regner, K. T.; Sellan, D. P.; Su, Z.; Amon, C. H.; McGaughey, A. J. H.; Malen, J. A. Broadband Phonon Mean Free Path Contributions to Thermal Conductivity Measured Using Frequency Domain Thermoreflectance. *Nat. Commun.* **2013**, *4*, 1640.

(11) Wilson, R. B.; Cahill, D. G. Anisotropic Failure of Fourier Theory in Time-Domain Thermoreflectance Experiments. *Nat. Commun.* **2014**, *5*, 1–11.

(12) Costescu, R. M.; Wall, M. A.; Cahill, D. G. Thermal Conductance of Epitaxial Interfaces. *Phys. Rev. B* **2003**, *67*, 054302.

(13) Cahill, D. G. Analysis of Heat Flow in Layered Structures for Time-Domain Thermoreflectance. *Rev. Sci. Instrum.* **2004**, *75*, 5119–5122.

(14) Minnich, A. J.; Johnson, J. A.; Schmidt, A. J.; Esfarjani, K.; Dresselhaus, M. S.; Nelson, K. A.; Chen, G. Thermal Conductivity Spectroscopy Technique to Measure Phonon Mean Free Paths. *Phys. Rev. Lett.* **2011**, *107*, 095901.

(15) Johnson, J. A.; Maznev, A. A.; Cuffe, J.; Eliason, J. K.; Minnich, A. J.; Kehoe, T.; Torres, C. M. S.; Chen, G.; Nelson, K. A. Direct Measurement of Room-Temperature Nondiffusive Thermal Transport Over Micron Distances in a Silicon Membrane. *Phys. Rev. Lett.* **2013**, *110*, 025901.

(16) Wilson, O. M.; Hu, X.; Cahill, D. G.; Braun, P. V. Colloidal Metal Particles as Probes of Nanoscale Thermal Transport in Fluids. *Phys. Rev. B* **2002**, *66*, 224301.

(17) Hu, M.; Hartland, G. V. Heat Dissipation for Au Particles in Aqueous Solution: Relaxation Time versus Size. *J. Phys. Chem. B* **2002**, *106*, 7029–7033.

(18) Banfi, F.; Juvé, V.; Nardi, D.; Dal Conte, S.; Giannetti, C.; Ferrini, G.; Del Fatti, N.; Vallée, F. Temperature Dependence of the Thermal Boundary Resistivity of Glass-Embedded Metal Nanoparticles. *Appl. Phys. Lett.* **2012**, *100*, 011902.

(19) Stoll, T.; Maioli, P.; Crut, A.; Rodal-Cedeira, S.; Pastoriza-Santos, I.; Vallée, F.; Del Fatti, N. Time-Resolved Investigations of the Cooling Dynamics of Metal Nanoparticles: Impact of Environment. *J. Phys. Chem. C* **2015**, *119*, 12757–12764.

(20) Park, J.; Cahill, D. G. Plasmonic Sensing of Heat Transport at Solid–Liquid Interfaces. *J. Phys. Chem. C* **2016**, *120*, 2814–2821.

(21) von Reppert, A.; Sarhan, R. M.; Stete, F.; Pudell, J.; Del Fatti, N.; Crut, A.; Koetz, J.; Liebig, F.; Prietzel, C.; Bargheer, M. Watching the Vibration and Cooling of Ultrathin Gold Nanotriangles by Ultrafast X-Ray Diffraction. *J. Phys. Chem. C* **2016**, *120*, 28894–28899.

(22) Hoogeboom-Pot, K. M.; Hernandez-Charpak, J. N.; Gu, X.; Frazer, T. D.; Anderson, E. H.; Chao, W.; Falcone, R. W.; Yang, R.; Murnane, M. M.; Kapteyn, H. C.; Nardi, D. A New Regime of Nanoscale Thermal Transport: Collective Diffusion Increases Dissipation Efficiency. *Proc. Natl. Acad. Sci.* **2015**, *112*, 4846–4851.

(23) Frazer, T. D.; Knobloch, J. L.; Hoogeboom-Pot, K. M.; Nardi, D.; Chao, W.; Falcone, R. W.;

Murnane, M. M.; Kapteyn, H. C.; Hernandez-Charpak, J. N. Engineering Nanoscale Thermal Transport: Size- and Spacing-Dependent Cooling of Nanostructures. *Phys. Rev. Appl.* **2019**, *11*, 1.

(24) Hu, Y.; Zeng, L.; Minnich, A. J.; Dresselhaus, M. S.; Chen, G. Spectral Mapping of Thermal Conductivity through Nanoscale Ballistic Transport. *Nat. Nanotechnol.* **2015**, *10*, 701–706.

(25) Zhang, H.; Hua, C.; Ding, D.; Minnich, A. J. Length Dependent Thermal Conductivity Measurements Yield Phonon Mean Free Path Spectra in Nanostructures. *Sci. Rep.* **2015**, *5*, 9121.

(26) Oyake, T.; Sakata, M.; Shiomi, J. Nanoscale Thermal Conductivity Spectroscopy by Using Gold Nano-Islands Heat Absorbers. *Appl. Phys. Lett.* **2015**, *106*, 073102.

(27) Beardo, A.; Knobloch, J. L.; Sendra, L.; Bafaluy, J.; Frazer, T. D.; Chao, W.; Hernandez-Charpak, J. N.; Kapteyn, H. C.; Abad, B.; Murnane, M. M.; Alvarez, F. X.; Camacho, J. A General and Predictive Understanding of Thermal Transport from 1D- And 2D-Confined Nanostructures: Theory and Experiment. *ACS Nano* **2021**, *15*, 13019–13030.

(28) Hu, M.; Petrova, H.; Hartland, G. V. Investigation of the Properties of Gold Nanoparticles in Aqueous Solution at Extremely High Lattice Temperatures. *Chem. Phys. Lett.* **2004**, *391*, 220–225.

(29) Plech, A.; Kotaidis, V.; Grésillon, S.; Dahmen, C.; von Plessen, G. Laser-Induced Heating and Melting of Gold Nanoparticles Studied by Time-Resolved x-Ray Scattering. *Phys. Rev. B* **2004**, *70*, 195423.

(30) Crut, A.; Maioli, P.; Del Fatti, N.; Vallée, F. Optical Absorption and Scattering Spectroscopies of Single Nano-Objects. *Chem. Soc. Rev.* **2014**, *43*, 3921–3956.

(31) Hu, M.; Novo, C.; Funston, A.; Wang, H.; Staleva, H.; Zou, S.; Mulvaney, P.; Xia, Y.; Hartland, G. V. Dark-Field Microscopy Studies of Single Metal Nanoparticles: Understanding the Factors That Influence the Linewidth of the Localized Surface Plasmon Resonance. *J. Mater. Chem.* **2008**, *18*, 1949–1960.

(32) Baida, H.; Mongin, D.; Christofilos, D.; Bachelier, G.; Crut, A.; Maioli, P.; Del Fatti, N.; Vallée, F. Ultrafast Nonlinear Optical Response of a Single Gold Nanorod near Its Surface Plasmon Resonance. *Phys. Rev. Lett.* **2011**, *107*, 057402.

(33) Ruijgrok, P. V; Zijlstra, P.; Tchebotareva, A. L.; Orrit, M. Damping of Acoustic Vibrations of Single Gold Nanoparticles Optically Trapped in Water. *Nano Lett.* **2012**, *12*, 1063–1069.

(34) Staleva, H.; Hartland, G. V. Vibrational Dynamics of Silver Nanocubes and Nanowires Studied by Single-Particle Transient Absorption Spectroscopy. *Adv. Funct. Mater.* **2008**, *18*, 3809–3817.

(35) Crut, A.; Maioli, P.; Del Fatti, N.; Vallée, F. Acoustic Vibrations of Metal Nano-Objects: Time-Domain Investigations. *Phys. Rep.* **2015**, *549*, 1–43.

(36) Medeghini, F.; Crut, A.; Gandolfi, M.; Rossella, F.; Maioli, P.; Vallée, F.; Banfi, F.; Del Fatti, N. Controlling the Quality Factor of a Single Acoustic Nanoresonator by Tuning Its Morphology. *Nano Lett.* **2018**, *18*, 5159–5166.

(37) Setoura, K.; Okada, Y.; Werner, D.; Hashimoto, S. Observation of Nanoscale Cooling Effects by Substrates and the Surrounding Media for Single Gold Nanoparticles under CW-Laser Illumination. *ACS Nano* **2013**, *7*, 7874–7885.

(38) Rouxel, R.; Diego, M.; Medeghini, F.; Maioli, P.; Rossella, F.; Vallée, F.; Banfi, F.; Crut, A.; Del

Fatti, N. Ultrafast Thermo-Optical Dynamics of a Single Metal Nano-Object. *J. Phys. Chem. C* **2020**, *124*, 15625–15633.

(39) Rouxel, R.; Diego, M.; Maioli, P.; Lascoux, N.; Vialla, F.; Rossella, F.; Banfi, F.; Vallée, F.; Del Fatti, N.; Crut, A. Electron and Lattice Heating Contributions to the Transient Optical Response of a Single Plasmonic Nano-Object. *J. Phys. Chem. C* **2021**.

(40) Mitiche, S.; Marguet, S.; Charra, F.; Douillard, L. Plasmonics of Regular Shape Particles, a Simple Group Theory Approach. *Nano Res.* **2020**, *13*, 1597–1603.

(41) Young, K. L.; Jones, M. R.; Zhang, J.; Macfarlane, R. J.; Esquivel-Sirvent, R.; Nap, R. J.; Wu, J.; Schatz, G. C.; Lee, B.; Mirkin, C. A. Assembly of Reconfigurable One-Dimensional Colloidal Superlattices Due to a Synergy of Fundamental Nanoscale Forces. *Proc. Natl. Acad. Sci.* **2012**, *109*, 2240–2245.

(42) Rodríguez-Fernández, J.; Pérez-Juste, J.; Mulvaney, P.; Liz-Marzán, L. M. Spatially-Directed Oxidation of Gold Nanoparticles by Au(III)-CTAB Complexes. *J. Phys. Chem. B* **2005**, *109*, 14257–14261.

(43) O'Brien, M. N.; Jones, M. R.; Kohlstedt, K. L.; Schatz, G. C.; Mirkin, C. A. Uniform Circular Disks With Synthetically Tailorable Diameters: Two-Dimensional Nanoparticles for Plasmonics. *Nano Lett.* **2015**, *15*, 1012–1017.

(44) Movsesyan, A.; Marguet, S.; Muravitskaya, A.; Béal, J.; Adam, P.-M.; Baudrion, A.-L. Influence of the CTAB Surfactant Layer on Optical Properties of Single Metallic Nanospheres. *J. Opt. Soc. Am. A* **2019**, *36*, C78.

(45) Arbouet, A.; Christofilos, D.; Del Fatti, N.; Vallée, F.; Huntzinger, J.; Arnaud, L.; Billaud, P.; Broyer, M. Direct Measurement of the Single-Metal-Cluster Optical Absorption. *Phys. Rev. Lett.* **2004**, *93*, 127401.

(46) Medeghini, F.; Rouxel, R.; Crut, A.; Maioli, P.; Rossella, F.; Banfi, F.; Vallée, F.; Del Fatti, N. Signatures of Small Morphological Anisotropies in the Plasmonic and Vibrational Responses of Individual Nano-Objects. *J. Phys. Chem. Lett.* **2019**, *10*, 5372–5380.

(47) Muskens, O. L.; Del Fatti, N.; Vallée, F. Femtosecond Response of a Single Metal Nanoparticle. *Nano Lett.* **2006**, *6*, 552–556.

(48) Gandolfi, M.; Crut, A.; Medeghini, F.; Stoll, T.; Maioli, P.; Vallée, F.; Banfi, F.; Del Fatti, N. Ultrafast Thermo-Optical Dynamics of Plasmonic Nanoparticles. *J. Phys. Chem. C* **2018**, *122*, 8655–8666.

(49) Ferrera, M.; Della Valle, G.; Sygletou, M.; Magnozzi, M.; Catone, D.; O'Keeffe, P.; Paladini, A.; Toschi, F.; Mattera, L.; Canepa, M.; Bisio, F. Thermometric Calibration of the Ultrafast Relaxation Dynamics in Plasmonic Au Nanoparticles. *ACS Photonics* **2020**, *7*, 959–966.

(50) Del Fatti, N.; Voisin, C.; Christofilos, D.; Vallée, F.; Flytzanis, C. Acoustic Vibration of Metal Films and Nanoparticles. *J. Phys. Chem. A* **2000**, *104*, 4321–4326.

(51) Hartland, G. V. Coherent Vibrational Motion in Metal Particles: Determination of the Vibrational Amplitude and Excitation Mechanism. *J. Chem. Phys.* **2002**, *116*, 8048–8055.

(52) Hartland, G. V. Optical Studies of Dynamics in Noble Metal Nanostructures. *Chem. Rev.* **2011**, *111*, 3858–3887.

(53) Dilhaire, S.; Pernot, G.; Calbris, G.; Rampnoux, J. M.; Grauby, S. Heterodyne Picosecond Thermoreflectance Applied to Nanoscale Thermal Metrology. *J. Appl. Phys.* **2011**, *110*, 114314.

(54) Collins, K. C.; Maznev, A. A.; Cuffe, J.; Nelson, K. A.; Chen, G. Examining Thermal Transport through a Frequency-Domain Representation of Time-Domain Thermoreflectance Data. *Rev. Sci. Instrum.* **2014**, *85*.

(55) Zhang, X.; Grigoropoulos, C. P. Thermal Conductivity and Diffusivity of Free-standing Silicon Nitride Thin Films. *Rev. Sci. Instrum.* **1995**, *66*, 1115–1120.

(56) Lee, S.-M.; Cahill, D. G. Heat Transport in Thin Dielectric Films. *J. Appl. Phys.* **1997**, *81*, 2590–2595.

(57) La Spina, L.; van Herwaarden, A. W.; Schellevis, H.; Wien, W. H. A.; Nenadovic, N.; Nanver, L. K. Bulk-Micromachined Test Structure for Fast and Reliable Determination of the Lateral Thermal Conductivity of Thin Films. *J. Microelectromechanical Syst.* **2007**, *16*, 675–683.

(58) Alam, M. T.; Manoharan, M. P.; Haque, M. A.; Muratore, C.; Voevodin, A. Influence of Strain on Thermal Conductivity of Silicon Nitride Thin Films. *J. Micromechanics Microengineering* **2012**, *22*, 045001.

(59) Bogner, M.; Hofer, A.; Benstetter, G.; Gruber, H.; Fu, R. Y. Q. Differential 3ω Method for Measuring Thermal Conductivity of AlN and Si3N4 Thin Films. *Thin Solid Films* **2015**, *591*, 267–270.

(60) Ftouni, H.; Blanc, C.; Tainoff, D.; Fefferman, A. D.; Defoort, M.; Lulla, K. J.; Richard, J.; Collin, E.; Bourgeois, O. Thermal Conductivity of Silicon Nitride Membranes Is Not Sensitive to Stress. *Phys. Rev. B* **2015**, *92*, 1–7.

(61) Cheng, C.; Fan, W.; Cao, J.; Ryu, S.-G.; Ji, J.; Grigoropoulos, C. P.; Wu, J. Heat Transfer across the Interface between Nanoscale Solids and Gas. *ACS Nano* **2011**, *5*, 10102–10107.

(62) Chen, S.; Moore, A. L.; Cai, W.; Suk, J. W.; An, J.; Mishra, C.; Amos, C.; Magnuson, C. W.; Kang, J.; Shi, L.; Ruoff, R. S. Raman Measurements of Thermal Transport in Suspended Monolayer Graphene of Variable Sizes in Vacuum and Gaseous Environments. *ACS Nano* **2011**, *5*, 321–328.

(63) Graczykowski, B.; El Sachat, A.; Reparaz, J. S.; Sledzinska, M.; Wagner, M. R.; Chavez-Angel, E.; Wu, Y.; Volz, S.; Wu, Y.; Alzina, F.; Sotomayor Torres, C. M. Thermal Conductivity and Air-Mediated Losses in Periodic Porous Silicon Membranes at High Temperatures. *Nat. Commun.* **2017**, *8*, 415.

(64) Schmidt, A. J.; Cheaito, R.; Chiesa, M. Characterization of Thin Metal Films via Frequency-Domain Thermoreflectance. *J. Appl. Phys.* **2010**, *107*, 024908.

(65) Koh, Y. K.; Cahill, D. G. Frequency Dependence of the Thermal Conductivity of Semiconductor Alloys. *Phys. Rev. B - Condens. Matter Mater. Phys.* **2007**, *76*, 1–5.

(66) Smith, A. N.; Hostetler, J. L.; Norris, P. M. Thermal Boundary Resistance Measurements Using a Transient Thermoreflectance Technique. *Microscale Thermophys. Eng.* **2000**, *4*, 51–60.

(67) Burzo, M. G.; Komarov, P. L.; Raad, P. E. Thermal Transport Properties of Gold-Covered Thin-Film Silicon Dioxide. *IEEE Trans. Components Packag. Technol.* **2003**, *26*, 80–88.

(68) Brown, D. B.; Bougher, T. L.; Cola, B. A.; Kumar, S. Oxidation Limited Thermal Boundary Conductance at Metal-Graphene Interface. *Carbon N. Y.* **2018**, *139*, 913–921.

(69) Hatam-Lee, S. M.; Jabbari, F.; Rajabpour, A. Interfacial Thermal Conductance between Gold and SiO 2 : A Molecular Dynamics Study. *Nanoscale Microscale Thermophys. Eng.* **2022**, *26*, 40–51.

(70) Juvé, V.; Scardamaglia, M.; Maioli, P.; Crut, A.; Merabia, S.; Joly, L.; Del Fatti, N.; Vallée, F. Cooling Dynamics and Thermal Interface Resistance of Glass-Embedded Metal Nanoparticles. *Phys. Rev. B* **2009**, *80*, 195406.

(71) Jeong, T.; Zhu, J.-G.; Chung, S.; Gibbons, M. R. Thermal Boundary Resistance for Gold and CoFe Alloy on Silicon Nitride Films. *J. Appl. Phys.* **2012**, *111*, 083510.

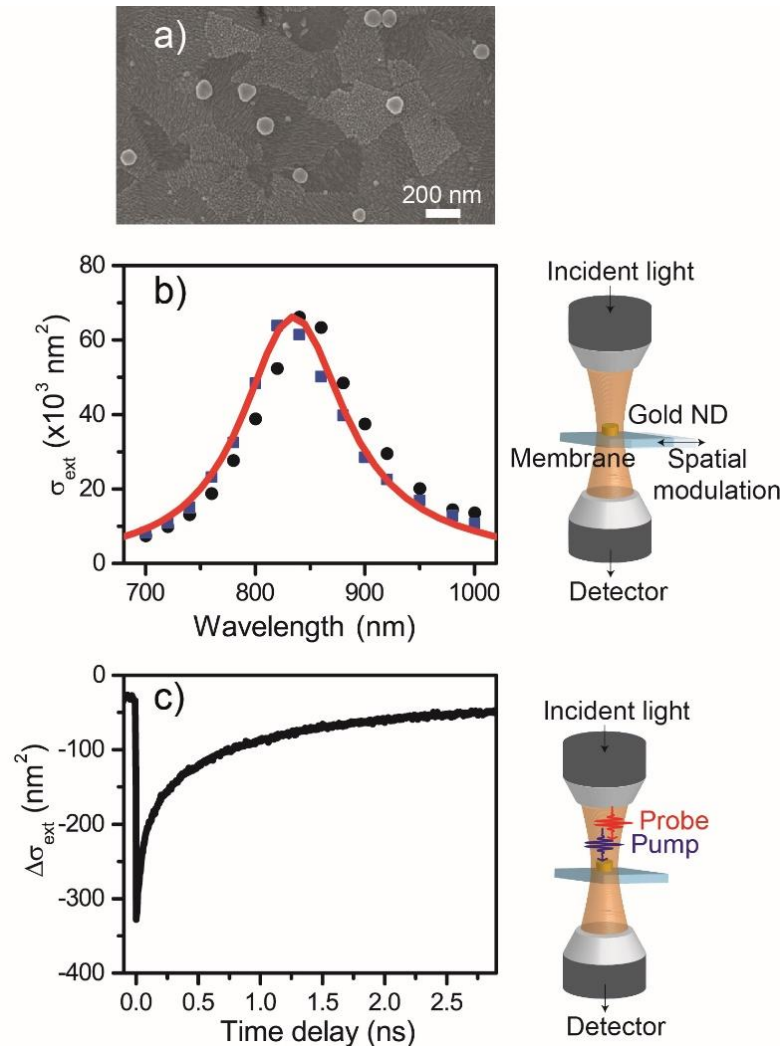

Figure 1. Electron microscopy characterization and single-particle optical spectroscopy of gold NDs. a) SEM image of the synthesized NDs. b) SMS-measured and FEM-modeled extinction spectra of a single gold ND deposited on a 40 nm thick silica membrane. The black circles and blue squares correspond to measurements performed with two orthogonal polarizations of the incident light. The red line corresponds to the result of a FEM simulation considering a circular ND with D=112 nm diameter and h=7.8 nm thickness. The principle of SMS is schematized on the right. c) Time-resolved extinction change measured on the same ND with pump-probe spectroscopy, using λ_{pp}= 405 nm and λ_{pr}= 810 nm pump and probe wavelengths, and F_{pp}= 2 J.m^{-2} pump fluence. The principle of single-particle optical spectroscopy is schematized on the right.

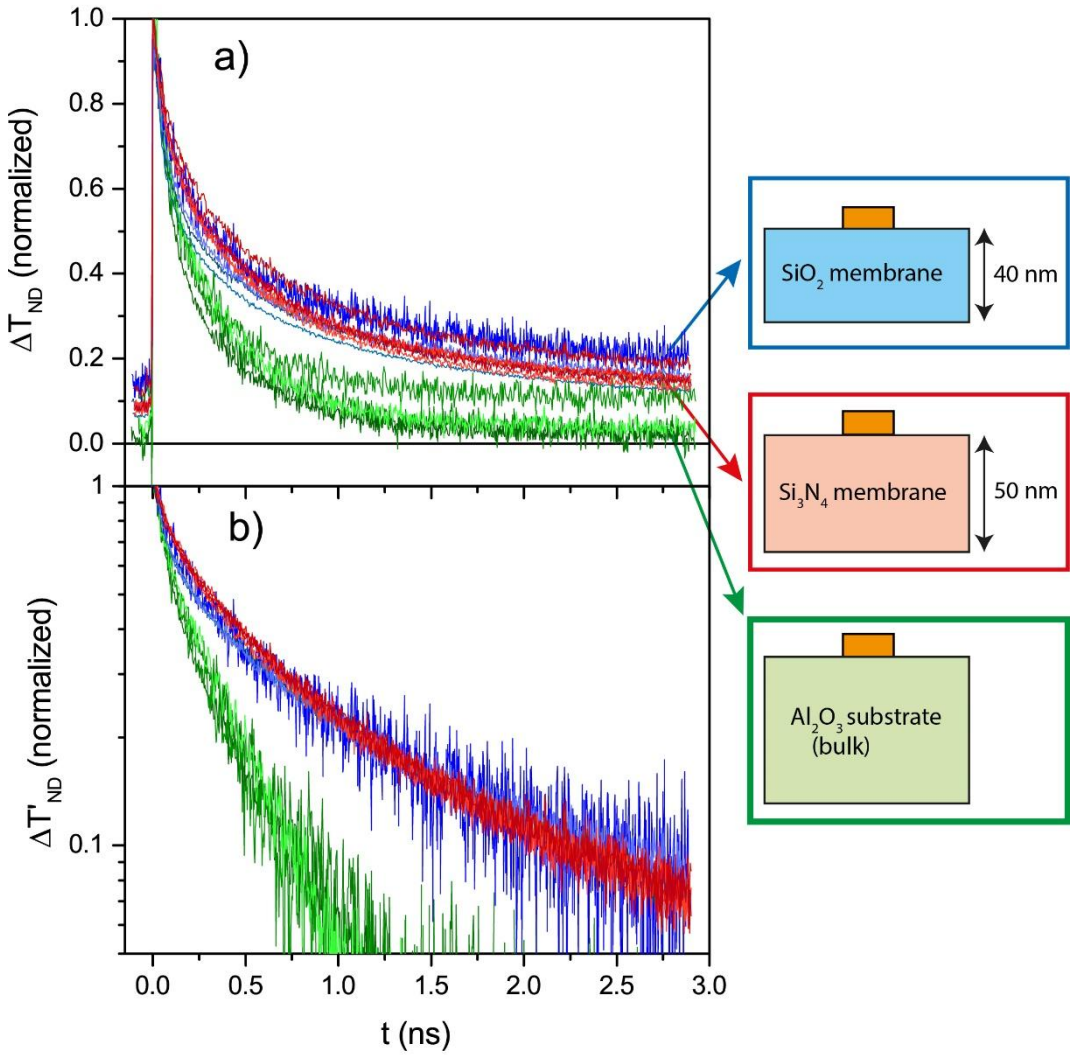

Figure 2. Comparison of the cooling dynamics measured for single gold NDs supported on different substrates. a) Normalized $\Delta T_{ND}(t)$ temperature rise dynamics measured on gold NDs deposited on a thick sapphire substrate (green traces), on a 40 nm thick silica membrane (blue traces) and on a 50 nm thick Si_3N_4 membrane (red traces). Each trace corresponds to a measurement on a distinct gold ND. b) Signals deduced from those of panel a) after subtraction of their average values at negative time delays $\Delta T'_{ND}(t) = \Delta T_{ND}(t) - \Delta T_{ND}(0^-)$ and normalization, presented on a logarithmic scale (same color code).

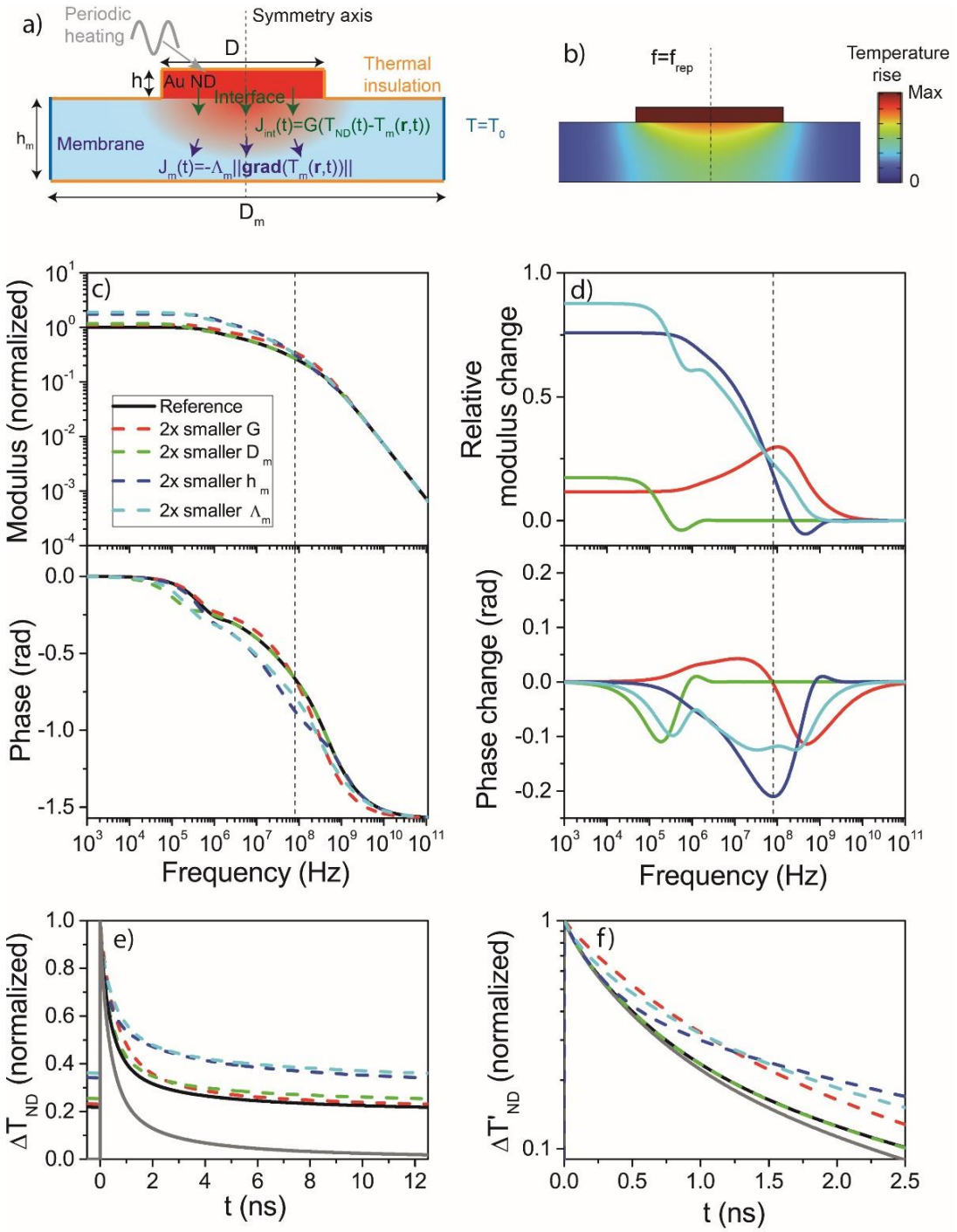

Figure 3. Numerical modeling of the thermal dynamics of a membrane-supported gold ND excited by a periodic pump pulse train. a) Schematic description of the FEM model used for computing the spatio-temporal temperature variations induced by a sinusoidal excitation of a gold ND supported on a thin membrane. b) Temperature rise (modulus) in and near the gold ND computed for excitation at the frequency $f=f_{rep}$=80 MHz. c) Frequency-dependent ND temperature rise induced by a sinusoidal ND excitation (modulus and phase of the frequency-domain response $\tilde{h}(f)$). The case of a D=100 nm, h=10 nm gold nanodisk supported on a h_m=40 nm, D_m= 2 µm silica membrane with a G=100 MW.m^{-2}.K^{-1} thermal conductance at their interface was first considered (plain black line). Simulations were then reproduced with h_m, D_m, Λ_m and G values reduced one by one by a factor 2 as compared to the reference situation (dashed colored lines, see legend). The vertical dashed line indicates the 80 MHz

repetition frequency in our experiments. d) Sensitivity of ND heating to h_m, D_m, Λ_m and G values, deduced from the computations shown in c) by calculating the associated relative modulus change and absolute phase change of ND heating (same color code as in c)). e) Normalized $\Delta T_{ND}(t)$ cooling dynamics deduced from the frequency calculations shown in c) for ND excitation by a periodic Dirac pulse train (same color code as in c). f) Normalized $\Delta T'_{ND}(t)$ cooling dynamics deduced from e). Note that modification of D_m (dashed green line) does not modify the $\Delta T'_{ND}(t)$ dynamics as compared to the reference case (plain black line). The computed cooling dynamics following ND excitation by a single pump pulse are also shown for comparison in panels e) and f) (plain gray line).

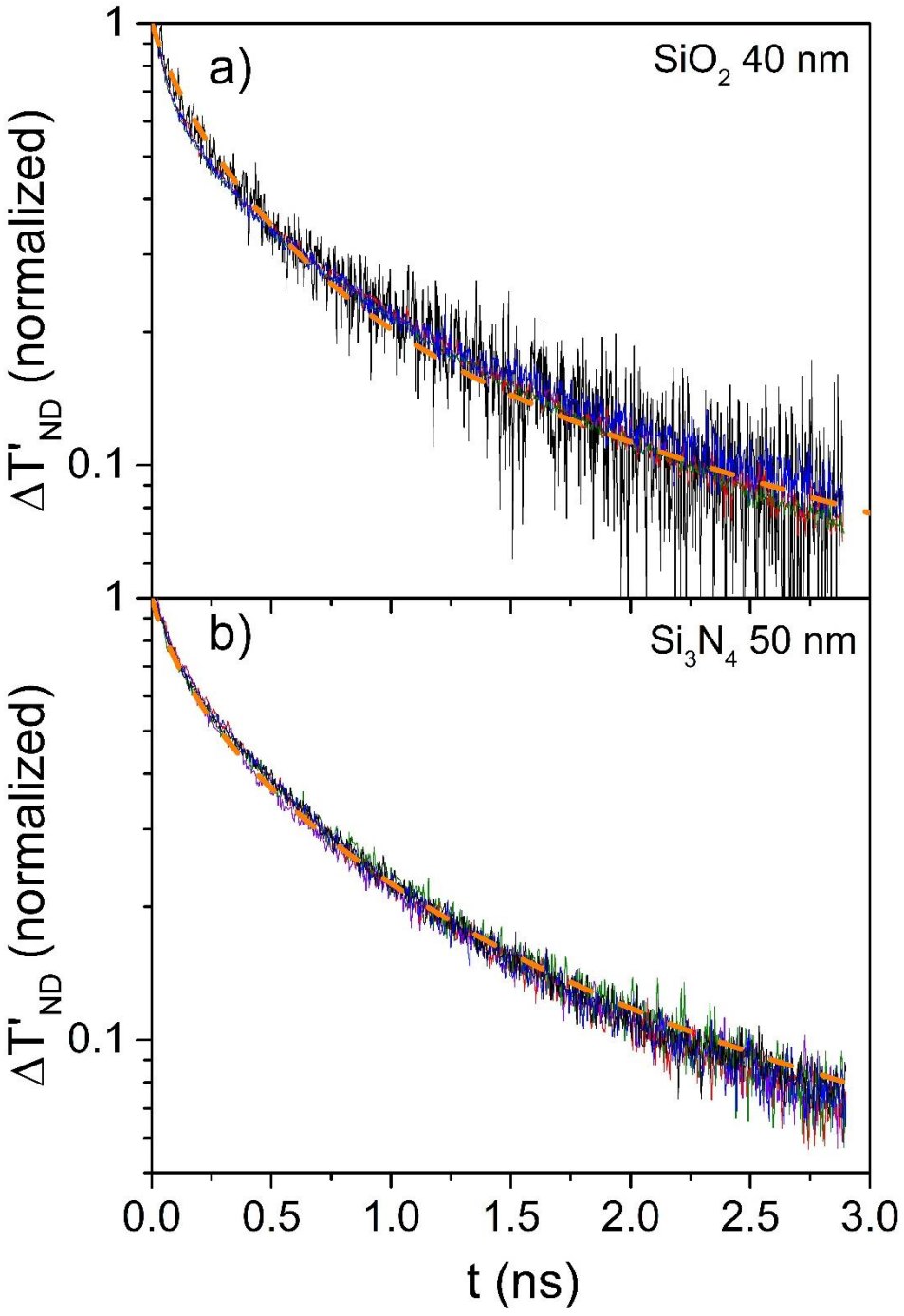

Figure 4. Comparison between measured and modeled cooling dynamics of gold NDs supported on a) SiO_2 and b) Si_3N_4 thin membranes (as indicated on each panel). The measured signals (plain lines) correspond to those of Figure 2b. The results of simulations based on the complete model described in the main text are shown as dashed orange lines. They were performed for a D=100 nm, h=10 nm gold ND, using G=120 $MW.m^{-2}.K^{-1}$ and bulk silica conductivity (Λ_m=1.4 $W.m^{-1}.K^{-1}$) in a) and G=150 $MW.m^{-2}.K^{-1}$ and Λ_m=1 $W.m^{-1}.K^{-1}$ for Si_3N_4 thermal conductivity in b).

TOC

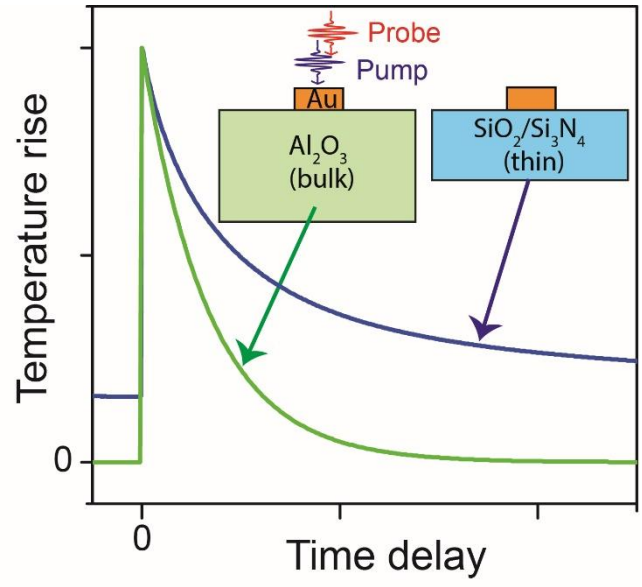
Probe
Pump
Au
Al_2O_3
(bulk)
SiO_2/Si_3N_4
(thin)
Temperature rise
0
0
Time delay